analytical chemistry

Technical Note

pubs.acs.org/ac

# Effect of Thermal Desorption Kinetics on Vapor Injection Peak Irregularities by a Microscale Gas Chromatography Preconcentrator

Jung Hwan Seo,[†,‡] Jing Liu,[†,⊥] Xudong Fan,[†,⊥] and Katsuo Kurabayashi*[,†,‡,§]

[†]Engineering Research Center for Wireless Integrated Microsensing and Systems (WIMS[2]), University of Michigan, Ann Arbor, Michigan 48109, United States

[‡]Department of Mechanical Engineering, University of Michigan, Ann Arbor, Michigan 48109, United States

[§]Department of Electrical Engineering and Computer Science, University of Michigan, Ann Arbor, Michigan 48109, United States

[⊥]Department of Biomedical Engineering, University of Michigan, Ann Arbor, Michigan 48109, United States

Supporting Information

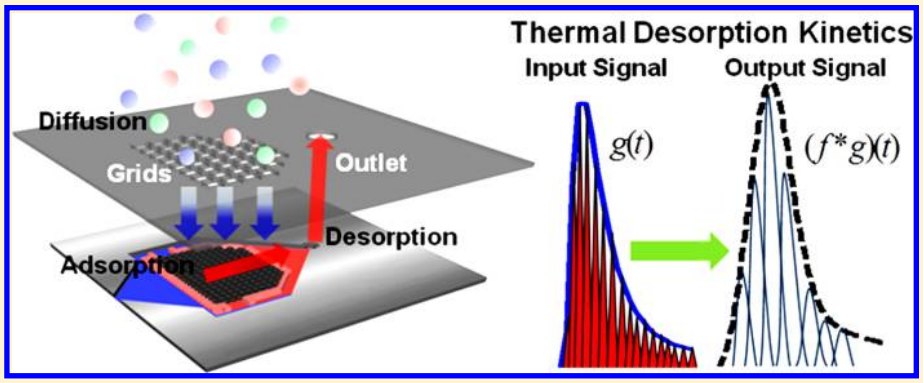


**ABSTRACT:** Microscale gas chromatography (μGC) is an emerging analytical technique for in situ analysis and on-site monitoring of volatile organic compounds (VOCs) in moderately complex mixtures. One of the critical subcomponents in a μGC system is a microfabricated preconcentrator (μ-preconcentrator), which enables detection of compounds existing in indoor/ambient air at low (~sub ppb) concentrations by enhancing their signals. The prevailing notion is that elution peak broadening and tailing phenomena resulting from undesirable conditions of a microfabricated separation column (μ-column) are the primary sources of poor chromatographic resolution. However, previous experimental results indicate that the resolution degradation still remains observed for a μ-column integrated with other μGC subcomponents even after setting optimal separation conditions. In this work, we obtain the evidence that the unoptimized μ-preconcentrator vapor release/injection performance significantly contributes to decrease the fidelity of μGC analysis using our state-of-the-art passive preconcentrator microdevice. The vapor release/injection performance is highly affected by the kinetics of the thermal desorption of compounds trapped in the microdevice. Decreasing the heating rate by 20% from the optimal rate of 90 °Cs$^{-1}$ causes a 340% increase in peak tailing as well as 70% peak broadening (30% peak height reduction) to the microscale vapor injection process.

Volatile organic compounds (VOCs), emanating from solids or liquids at finite vapor pressure, may cause adverse health risks from breathing indoor/ambient air. A gas chromatographic system (GC) is widely used to measure and monitor VOCs. It is often challenging to obtain on-site data in indoor or ambient air due to high costs, high power requirements, and large sizes. Therefore, in situ analysis and on-site monitoring of VOCs in moderately complex mixtures require the use of a microscale gas chromatographic (μGC) system that can serve as a highly portable microanalytical tool. The valuable applications of a μGC system include point-of-care medical diagnostics,[1−3] homeland security, and worker exposure assessment. A μGC system generally comprises the following three essential components, all of which are fluidically interconnected and microfabricated: (1) a preconcentrator, (2) a separation column, and (3) a detector.[4−9] In particular, microfabricated preconcentrator devices (μ-preconcentrators)[10−12] play a critical role to enhance the detection sensitivity and separation resolution of μGC systems; they trap and concentrate VOCs initially at low concentrations with integrated adsorbents and inject high-intensity sharp plugs of the trapped VOCs via rapid thermal desorption to a downstream GC column.

A particular challenge to a μGC system is to maintain high chromatographic separation resolution with a microfabricated column (μ-column). The relatively short (~3 m) μ-column length is highly susceptible to adverse effects by irregular elution peak shapes. Peak broadening and tailing are shape

**Received:** March 17, 2012
**Accepted:** July 9, 2012
**Published:** July 9, 2012

   dx.doi.org/10.1021/ac300755d | *Anal. Chem.* 2012, 84, 6336−6340

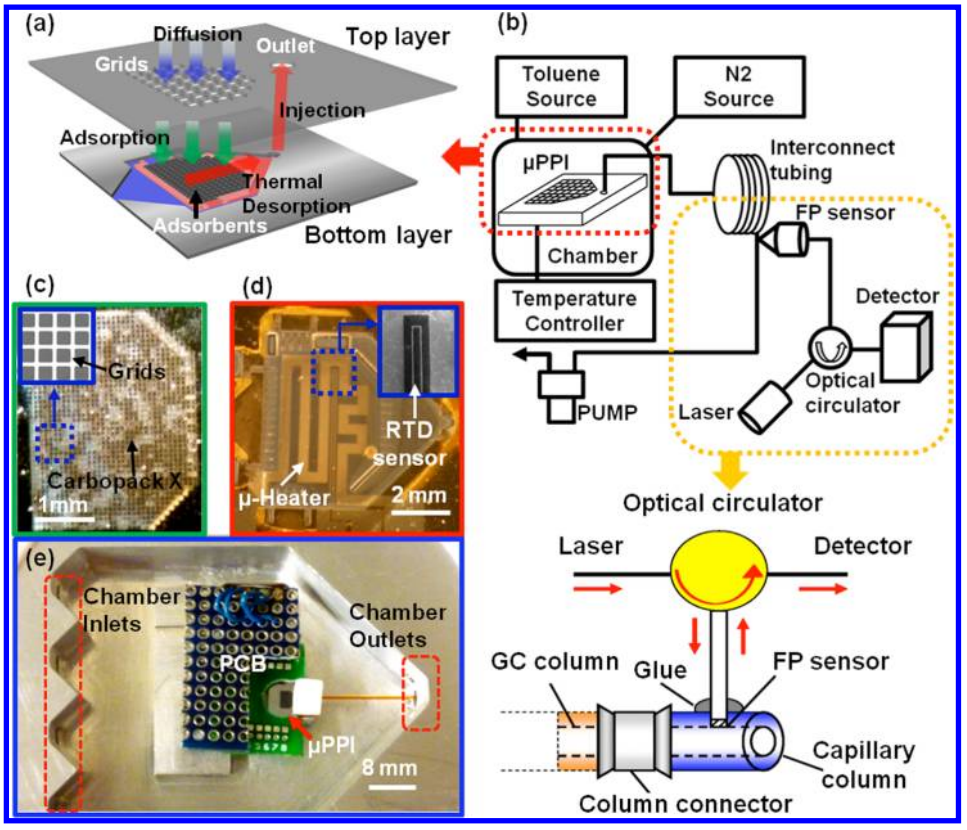


**Figure 1.** (a) Conceptual diagram of the μPPI showing the diffusional sampling and thermal desorption processes. (b) Schematic of the test setup incorporating a Fabry-Pérot (FP) optical gas sensor that was used to characterize the μPPI performance for real-time desorption and injection of toluene. (c) Optical image showing the top layer of the μPPI with diffusion channel grids and see-through image of Carbopack X beads packed underneath. (d) Optical image of the microheater and RTD sensor on the backside of the bottom layer of the μPPI. (e) Optical image of the μPPI mounted in the exposure chamber with its PCB packaging.

irregularities that seriously reduce the GC separation resolution. Often, pre- and post-treatments of a polymeric stationary phase material deposited inside a μ-column are performed to reduce peak broadening and tailing of VOCs.[13−17] For example, previous studies[4,18] demonstrated that the surface treatment of a stationary phase in a stand-alone μ-column yielded a symmetric elution peak shape leading to stable GC separation performance, but surprisingly, significant peak tailing phenomena together with peak broadening were found to recur after the surface-treated μ-column was integrated with other μGC components.[4,19] This peak shape degradation has been a persistent issue observed upon μGC system integration and still remains unsolved. Now, we address the following question in this study: what is the additional source of peak broadening and tailing in a μGC system? Here, we hypothesize that the peak broadening and tailing in a μGC system are also highly attributed to a nonideal vapor injection process driven by a μ-preconcentrator connected to the μ-column.

In this Technical Note, we investigate the effect of the vapor injection performance of a μ-preconcentrator on analyte peak shape irregularities, specifically, in terms of peak tailing and broadening. Our study aims to establish a good understanding of the thermal desorption kinetics during the vapor injection process and its influence on a μGC system. To this end, we first develop a theoretical model enabling us to quantitatively predict the vapor release/injection profiles in a μ-preconcentrator device.[12,20−22] To experimentally validate our model, we use our state-of-the-art μ-preconcentrator, named the "microfabricated passive vapor preconcentrator/injector (μPPI)", capable of achieving the high-speed thermal desorption with a low power of ∼1 W because of its low thermal mass.[23] Using the μPPI, we explore the changes in injection peak tailing and broadening by intentionally decreasing the device's heating rate during the thermal desorption process. In this study, toluene is used as the test vapor. Toluene serves as a representative example of VOCs that are highly relevant to indoor air quality monitoring, environmental pollution, toxic human exposure, and disease diagnosis.[1−3,24] The volatility and diffusivity of toluene are close to the median values over a broad range of these VOCs.[25] The knowledge obtained by our theoretical and experimental investigations here provides an answer to the aforementioned conundrum through validating our hypothesis and guides us in developing a high-performance μGC technology.

## MATERIALS AND METHODS

**Device Design and Fabrication.** The μPPI was originally designed on the basis of the classical Fickian diffusion theory, heat transfer, and fluid dynamics. The device consists of two layer structures (Figure 1a): the top layer incorporates vertical square diffusion channel grids for passive VOC sampling from air, and the bottom layer contains a membrane cavity structure with tapered entrance/exit on its two sides, pillar structures to retain the graphitized carbon beads inside, and a meander-line Ti/Pt microheater and a resistance temperature detector (RTD) on its backside. As the first step of the device operation, the graphitized carbon (Carbopack X) beads on the cavity floor of the device adsorbed VOCs. These VOCs diffused


dx.doi.org/10.1021/ac300755d | Anal. Chem. 2012, 84, 6336−6340

into the cavity through the diffusion channel grids with no power requirements. Subsequently, the device was heated to thermally release the captured VOCs and to inject them to a downstream GC system with a carrier gas flow driven by a miniature pump. In our previous study,[23] the μPPI was fabricated using silicon micromachining and Au eutectic water bonding. The device achieved a sampling rate of ~9.1 mL/min by means of the passive diffusion process at a carrier gas flow rate of 50 mL/min. The low thermal mass of the device allows us to control the heating rate of the integrated microheater during the thermal desorption of VOCs with high sensitivity.

**Experimental Setup.** To characterize the vapor desorption/injection performance of the μPPI, we modified a custom-made exposure chamber setup developed in our previous study[23] and characterized the injection peak signals generated by the device after sampling of 1 ppm toluene for 90 min. (Figure 1b). The modified setup incorporated a Fabry-Perót (FP) gas sensor[26−28] built in a stationary phase-free inert tubing of 50 cm in length and 0.23 cm in internal diameter. The inert interconnect tubing was necessary to retain the original injection profile with minimum band dispersion at the detection point. A relatively high $N_2$ carrier gas flow rate of 10 mL/min was used to minimize the height equivalent to a theoretical plate in the tubing (see Figure S1 in Supporting Information). Using the FP gas sensor, we were able to obtain the real-time vapor signal at this flow rate, which is not typically allowed by the conventional GC/flame ionization detector (FID) system.

**Transient Thermal Model.** We developed a heat transfer model to quantitatively predict the thermal response of the μPPI. Heat transfer equations were obtained from applying energy balance to each of the control volumes (CVs) assigned to several subsegments of the device structure (see Figure S2a in Supporting Information). The equations accounted for changes in energy storage and heat transfer due to conduction and convection associated with the CVs. The contribution of radiation was estimated to be less than 1% of the total heat transfer and was neglected in our model. Because of the high thermal conductivity of the structural materials of the device and the adsorbent materials, we assumed an isothermal condition for each CV. This allowed us to apply the lumped thermal capacitance method to predict the temperature of each CV. The simultaneous thermal equations are given in Section III of the Supporting Information. We obtained the transient temperature profile of each CV by solving simultaneous heat transfer equations (see Section III in Supporting Information).

**Vapor Desorption Kinetics.** We theoretically obtained the adsorption capacity of the μPPI from the adsorption isotherm, a theoretical curve representing the equilibrium mass of vapor adsorbed per adsorbent mass as a function of vapor concentration at a given temperature $T$. Among existing isotherm models, the Dubinin−Radushkevich−Kaganer (DRK) model is appropriate for the nonporous Carbopack X[12,20−22] used for the device. The DRK model is given as:

$$N_a = N_{am-DRK}\exp\left[-\left(\left(\frac{RT}{\beta E_0}\right)\ln\left(\frac{p}{p_{sat}}\right)\right)^2\right] \quad (1)$$

where $N_a$ is the molar amount adsorbed (mmol/g) and $N_{am-DRK}$ is the monolayer capacity (mmol/g) of the adsorbent, $\beta$ is the affinity coefficient of the adsorbent, $E_0$ is the adsorption energy, $p$ is the partial pressure of the vapor, and $p_{sat}$ is the saturation vapor pressure of the adsorbate at the test temperature. All parameters in the equation for toluene and Carbopack X are obtained experimentally and derived from published polarizability data.[12,29,30] The parameter values are given in Table S2, Supporting Information.

The partial pressure $p$ (mmHg) and saturation vapor pressure $p_{sat}$ (mmHg) of toluene can be obtained as functions of the adsorbent temperature $T$ from the ideal gas law and Antoine equation, respectively, and are given by:[31]

$$p = \frac{nRT}{V} \quad (2)$$

$$p_{sat} = 10^{\left(6.95464-\frac{1344.8}{T+219.482}\right)} \quad (3)$$

where $n$ is the number of moles of gas and $V$ is the volume of gas used during desorption, respectively.

Now, we substituted (a) the temperature profile of the adsorbent (i.e., Carbopack X) $T_2(t)$ as a function of time in eq S2 (Supporting Information), (b) the partial pressure in eq 2, and (c) the saturation vapor pressure of toluene at the temperature of $T_2$ in eq 3 into eq 1. We subsequently obtained the total amount of the vapor released from the adsorbent at a given time during the thermal desorption process by subtracting the real-time adsorption capacity $N_a(T(t))$ from the initial capacity at room temperature $N_a(T(0))$. Thus, the real-time cumulative desorption profile $N_{des}(t)$ is expressed as:

$$N_{des}(t) = N_a(T(0)) - N_{am-DRK}\exp\left[-\left(\left(\frac{RT_2(t)}{\beta E_0}\right)\ln\left(\frac{nRT_2(t)}{V\cdot 10^{\left(6.95464-\frac{1344.8}{T_2(t)+219.482}\right)}}\right)\right)^2\right] \quad (4)$$

**Vapor Peak Prediction.** Once vapors are desorbed from the adsorbent, these are immediately injected to a downstream component by a continuous suction air stream. Golay and Spangler developed kinetic models that predict the elution profile of VOCs leading to the band broadening in the moving phase.[32−34] The simplified Golay and Spangler equation (eq S16 in the Supporting Information) describes band dispersion in the inert interconnect tubing with a circular cross-section.[34] Assuming that the elution profile is the normal distribution and the injection pulse is the delta function, the standard deviation $\sigma$ of the vapor peak profile can be obtained as a function of the vapor retention time to elute ($t_r$), the height equivalent to a theoretical plate ($H$), and the column length ($L$) (see eq S17 in Supporting Information). Using eqs S16−S17 (Supporting Information), we theoretically predicted the normalized chromatographic peak band signal $f(t)$ resulting from a delta-function injection pulse. Substituting the values of the variables given in Table S2 into eqs S16−S17 (Supporting Information) yielded an expected standard deviation $\sigma$ of 0.69 s. This number was applied in the expression for $f(t)$ (given by eq S15 in Supporting Information) to theoretically obtain the elution profile of toluene with respect to a delta function injection profile.

The real-time injection profile of the target vapor $g(t)$ at the exit of the μPPI was obtained by taking the time-derivative of eq 4 (see Figure S3a in Supporting Information). Then, we calculated the theoretical peak band signal by taking the convolution of $g(t)$ and its impulse response corresponding to


dx.doi.org/10.1021/ac300755d | Anal. Chem. 2012, 84, 6336−6340

the normalized elution profile $f(t)$ (see Figure S3b in Supporting Information), which is given by

$$(f^*g)(t) = \int_{-\infty}^{\infty} f(\tau)g(t-\tau)\,d\tau \quad (5)$$

The formulation in eq 5 allowed us to predict the band signal characteristics of the vapor peak detected by the FP optical gas sensor, including the tailings, height, and full width at half-maximum (fwhm). All of these predicted band signal characteristics were directly compared to experimental results.

## RESULTS AND DISCUSSION

**Thermal Desorption Behavior.** Our theoretical model coupled the thermal equations predicting the real-time adsorbent surface temperature with the modified DRK equation. Assuming no sample loss, this heat transfer-desorption hybrid model enabled us to estimate the cumulative total mass of the vapor released from the $\mu$PPI by the transient thermal desorption process. Then, we performed tests to explore the correlation between the heating duration and the desorption kinetics (Figure 2). Toluene was first loaded to the $\mu$PPI by passive sampling for 15 min at the concentration of 1 ppm. The total mass of the toluene released by the subsequent thermal desorption process was measured for various heating durations by the downstream GC/FID (see Section I in the Supporting Information). We repeated tests for an additional 2 different concentrations of 350 and 270 ppb in order to thoroughly understand the desorption behavior of toluene within the $\mu$PPI and validate our analytical model. During the initial sampling process, the amounts of 496 ng, 175 ng, and 140 ng were sampled for 1 ppm, 350 ppb, and 270 ppb, respectively. Figure 2 shows that the predictions from the coupled thermal desorption kinetic model agree with the experimental results with a ± 10% error. Both the theoretical prediction and the experimental results indicate that the desorption process completes the release of 90% of the total mass of the sampled toluene within 3 s, which obviously results from the rapid thermal response of the $\mu$PPI. The quantitative characterization of the transient toluene desorption behavior successfully validated our model.

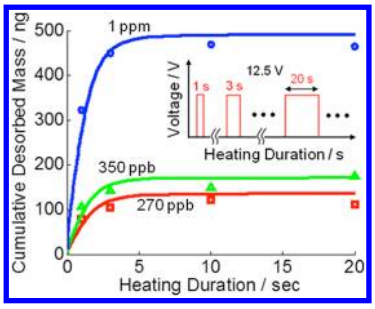


**Figure 2.** Theoretical and experimental plots of the total cumulative mass of toluene released from the $\mu$PPI by thermal desorption as a function of heating duration. They are given for toluene originally sampled for 15 min at 3 different concentrations of 270 ppb (red), 350 ppb (green), and 1 ppm (blue). The red squares (□), green triangles (△), blue circles (o) represent experimental data points obtained for different heating durations. The red, green, blue solid lines are the theoretical predictions at 270 ppb, 350 ppb, and 1 ppm, respectively. The inset shows the input voltage profiles applied to the microheater for a varying duration (i.e., heating duration) ranging from 1 to 20 s. All of the off-state periods between the adjacent heating cycles involve sampling, desorption/injection, and cleaning processes.

**Effect of Heating Rate on Peak Shape Irregularities.** Subsequently, we studied the effect of the heating rate of the $\mu$PPI on the injection peak band broadening. Figure 3a shows the theoretically predicted injection peak band signals at 3 different heating rate conditions of 90 °C·s$^{-1}$, 80 °C·s$^{-1}$, and 70 °C·s$^{-1}$ and those experimentally detected signals for the corresponding conditions. The higher heating rate is obviously more desirable for the peak intensity enhancement. There exists, however, the upper bound for the heating rate to prevent the device from breaking down due to a thermal shock (see Figure S6 in Supporting Information). To avoid the device failure, we selected the heating rate of 90 °C·s$^{-1}$ as the upper bound. We intentionally decreased the heating rate from 90 °C·s$^{-1}$ to 70 °C·s$^{-1}$ to observe changes in the vapor peak signal. The decrease in the heating rate by 20% from the upper bound of 90 °Cs$^{-1}$ to 70 °Cs$^{-1}$ yielded an increase in the fwhm by more than 70% by the model prediction and by 65% by the experiment as shown in Figure 3a,c. Also, this decrease in the heating rate reduced the peak height by 26% by the model prediction and by 30% by the experiment (Figure 3a). From the transient vapor signal profiles, we quantified the peak tailing

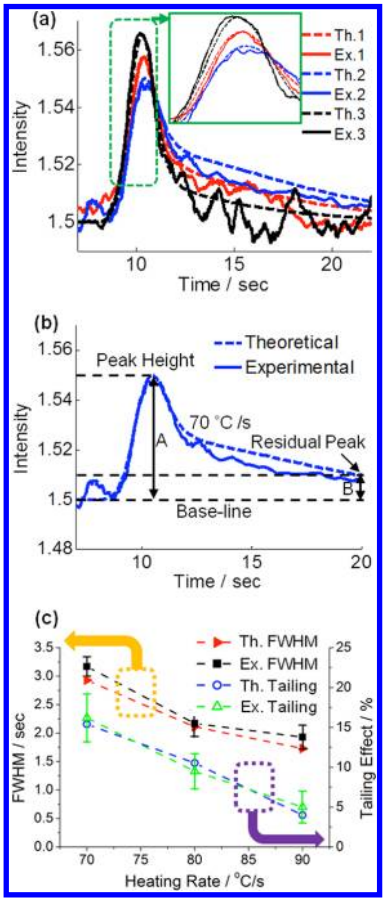


**Figure 3.** (a) Theoretical and experimental plots of the injection peak band profile of toluene generated by the $\mu$PPI at different heating rates of 90 °C·s$^{-1}$ (black), 80 °C·s$^{-1}$ (red), and 70 °C·s$^{-1}$ (blue). (b) Plots of the theoretical and experimental injection peak band profiles of toluene at the heating rate of 70 °C·s$^{-1}$. These plots clearly show injection peak tailings affected by the heating rate. (c) fwhm values and quantified injection peak tailing effect at different heating rates of 70 °C·s$^{-1}$, 80 °C·s$^{-1}$, and 90 °C·s$^{-1}$.


dx.doi.org/10.1021/ac300755d | Anal. Chem. 2012, 84, 6336−6340

effect by taking the ratio of the maximum peak height (A) to the residual peak height (B) (Figure 3b) and compared the experimental value to that of the theoretical curve. The use of the stationary-phase free tubing between the $\mu$PPI and the FP sensor removed the possibility of peak tailing caused by the nonequilibrium interaction between the mobile and the stationary phase in a conventional capillary column. We chose $t$ = 20 s in Figure 3a as the reference time point at which the residual peak height was determined. This decrease in the heating rate also caused a 340% increase in peak tailing (380% by the theory) to the microscale vapor injection process (Figure 3c). The result clearly validated our original working hypothesis.

## CONCLUSIONS

This note presents the first study quantitatively correlating thermal desorption at a microfabricated preconcentrator to injection peak shape irregularities in microscale gas chromatography. Two primary contributions of this study include: (1) developing the temperature-dependent desorption kinetic model, which is capable of quantitatively predicting the analyte injection vapor peak profile by a $\mu$-preconcentrator and (2) theoretically and experimentally proving that a nonideal thermal desorption condition is considerably responsible for injection vapor peak broadening and tailing by a $\mu$-preconcentrator. Accounting for both transient heat transfer and temperature-dependent vapor desorption kinetics, our analytical model well predicts the variation in the real-time vapor injection peak shape with the device heating profile. Our study quantitatively indicates that a rapid vapor desorption process is critically important to achieve high separation resolution in a $\mu$GC system. Thus, setting the heating profile of a $\mu$-preconcentrator at a sufficiently high temperature-rise rate while carefully avoiding thermal shock to the device is crucial to improve the peak capacity and sensitivity of the $\mu$GC analysis.

## ASSOCIATED CONTENT

### Supporting Information

Additional information as noted in text. This material is available free of charge via the Internet at http://pubs.acs.org.

## AUTHOR INFORMATION

### Corresponding Author

*E-mail: katsuo@umich.edu. Fax:+1-734-647-3170. Tel: 1-734-615-5211.

### Notes

The authors declare no competing financial interest.

## ACKNOWLEDGMENTS

The authors would like to thank Edward T. Zellers for assistance in device design. This work was supported by the Engineering Research Centers Program of the National Science Foundation under Award Number ERC-9986866 and NIOSH Pilot Project Research Training Program (PPRT).

## REFERENCES

(1) Phillips, M.; Cataneo, R. N.; Cummin, A. R. C.; Gagliardi, A. J.; Gleeson, K.; Greenberg, J.; Maxfield, R. A.; Rom, W. N. *Chest* **2003**, *123*, 2115−2123.
(2) Phillips, M.; Gleeson, K.; Hughes, J. M. B.; Greenberg, J.; Cataneo, R. N.; Baker, L.; McVay, W. P. *Lancet* **1999**, *353*, 1930−1933.
(3) Libardoni, M.; Stevens, P. T.; Waite, J. H.; Sacks, R. *J. Chromatogr., B* **2006**, *842*, 13−21.
(4) Kim, S. K.; Chang, H.; Zellers, E. T. *Anal. Chem.* **2011**, *83*, 7198−7206.
(5) Lu, C.-J.; Steinecker, W. H.; Tian, W.-C.; Agah, M.; Potkay, J. A.; Oborny, M. C.; Nichols, J. M.; Chan, H. K. L.; Driscoll, J.; Sacks, R. D.; Pang, S. W.; Wise, K. D.; Zellers, E. T. *Lab Chip* **2005**, *5*, 1123−1131.
(6) Zampolli, S.; Elmi, I.; Mancarella, F.; Betti, P.; Dalcanale, E.; Cardinali, G. C.; Severi, M. *Sens. Actuators, B* **2009**, *141*, 322−328.
(7) Lewis, P. R.; Manginell, R. P.; Adkins, D. R.; Kottenstette, R. J.; Wheeler, D. R.; Sokolowski, S. S.; Trudell, D. E.; Byrnes, J. E.; Okandan, M.; Bauer, J. M.; Manley, R. G.; Frye-Mason, G. C. *IEEE Sens. J.* **2006**, *6*, 784−795.
(8) Zellers, E. T.; Serrano, G.; Chang, H.; Amos, L. K. *IEEE Technical Digest Transducers' 11*, Beijing, China, June 5−9, 2011; Institute of Electrical and Electronics Engineers; pp 2082−2085.
(9) Kim, H.; Steinecker, W. H.; Reidy, S.; Lambertus, G. R.; Astle, A. A.; Najafi, K.; Zellers, E. T.; Bernal, L. P.; Washabaugh, P. D.; Wise, K. D. *IEEE Technical Digest Transducers' 07*, Lyon, France, June 10−15, 2007; Institute of Electrical and Electronics Engineers; pp 1505−1508.
(10) Manginell, R. P.; Adkins, D. R.; Moorman, M. W.; Hadizadeh, R.; Copic, D.; Porter, D. A.; Anderson, J. M.; Hietala, V. M.; Bryan, J. R.; Wheeler, D. R.; Pfeifer, K. B.; Rumpf, A. *J. Microelectromech. Syst.* **2008**, *17*, 1396−1407.
(11) Camara, E. H. M.; Breuil, P.; Briand, D.; Guillot, L.; Pijolat, C.; de Rooij, N. F. *Sens. Actuators, B* **2010**, *148*, 610−619.
(12) Veeneman, R. A. Ph.D. thesis, University of Michigan, Ann Arbor, Michigan, 2009.
(13) Lu, C-J.; Zellers, E. T. *Anal. Chem.* **2001**, *73*, 3449−3457.
(14) Giddings, J. C. *Anal. Chem.* **1963**, *35*, 1999−2002.
(15) Cieplinski, E. W. *Anal. Chem.* **1963**, *35*, 256−257.
(16) Grushka, E.; Myers, M. N.; Schettler, P. D.; Giddings, J. C. *Anal. Chem.* **1969**, *41*, 889−892.
(17) Samuelsson, J.; Franz, A.; Stanley, B. J.; Fornstedt, T. *J. Chromatogr., A* **2007**, *1163*, 177−189.
(18) Serrano, G.; Reidy, S. M.; Zellers, E. T. *Sens. Actuators, B* **2009**, *141*, 217−226.
(19) Kim, S. K.; Burris, D. R.; Chang, H.; Bryant-Genevier, J.; Zellers, E. T. *Environ. Sci. Technol.* **2012**, *46*, 6065−6072.
(20) Stoeckli, F.; López-Ramón, M. V.; Moreno-Castilla, C. *Langmuir* **2001**, *17*, 3301−3306.
(21) Mourão, P. A. M.; Carrott, P. J. M.; Ribeiro Carrott, M. M. L. *Carbon* **2006**, *44*, 2422−2429.
(22) Hugi-Cleary, D.; Stoeckli, F. *Carbon* **2000**, *38*, 1309−1313.
(23) Seo, J. H.; Kim, S. K.; Zellers, E. T.; Kurabayashi, K. *Lab Chip* **2012**, *12*, 717−724.
(24) Kirman, C. R.; Aylward, L. L.; Blount, B. C.; Pyatt, D. W.; Hays, S. M. *J. Exposure Sci. Environ. Epidemiol.* **2011**, *22*, 24−34.
(25) Nelson, G. O. *Gas Mixtures: Preparation and Control*; CRC Press: Boca Raton, FL, 1992.
(26) Liu, J.; Sun, Y.; Fan, X. *Optics Express* **2009**, *17*, 2731−2738.
(27) Liu, J.; Sun, Y.; Howard, D. J.; Frye-Mason, G.; Thompson, A. K.; Ja, S.-J.; Wang, S.-K.; Bai, M.; Taub, H.; Almasri, M.; Fan, X. *Anal. Chem.* **2010**, *82*, 4370−4375.
(28) Liu, J.; Gupta, N. K.; Wise, K. D.; Gianchandani, Y. B.; Fan, X. *Lab Chip* **2011**, *11*, 3487−3492.
(29) Noll, K. E.; Wang, D.; Shen, T. *Carbon* **1989**, *27*, 239−245.
(30) Wood, G. O. *Carbon* **1992**, *30*, 593−599.
(31) Surhone, L. M.; Tennoe, M. T.; Henssonow, S. F. *Antoine equation*; Academia, VDM Publishing: Saarbrücken, Germany, 2010.
(32) Golay, M. J. E. *J. Chromatogr.* **1981**, *216*, 1−8.
(33) Giddings, J. C.; Chang, J. P.; Myers, M. N.; Davis, J. M.; Caldwell, K. D. *J. Chromatogr.* **1983**, *255*, 359.
(34) Spangler, G. E. *J. Microcolumn Sep.* **2001**, *13*, 285−292.